HRTEM, TSC and broadband dielectric spectroscopy of a discotic liquid crystal

E. Dantras,*[a] J. Dandurand,[a] C. Lacabanne,[a] L. Laffont,[b] J. M. Tarascon,[b] S. Archambeau,[c] I. Seguy,[c] P. Destruel,[c] H. Bock[d] and S. Fouet[d]

[a] *Laboratoire de Physique des Polymères, CIRIMAT, Université Paul Sabatier, Toulouse Cedex 04 31062, France. E-mail: dantras@cict.fr*
[b] *Laboratoire de Réactivité et Chimie des Solides, Université Jules Vernes, Amiens 80000, France*
[c] *Laboratoire de Génie Electrique, Université Paul Sabatier, France*
[d] *Centre de Recherche Paul Pascal, Bordeaux, France*

Due to its molecular configuration, Pyrene 1,3,6,8-tetracarboxylic *rac*-2-ethyl hexyl ester exhibits a mesomorphic phase at room temperature. High resolution transmission electron microscopy (HRTEM) of samples with various thermal history yield important results on discotic liquid crystal nanostructure. The evolution of the molecular organisation with the temperature has been determined by differential scanning calorimetry (DSC). The physical structure of this columnar liquid crystal is shown by dynamic dielectric spectroscopy (DDS) along a broad temperature and frequency range. As this liquid crystal is used as film electronic devices, the thermostimulated micro-technique (μ-TSC) has been improved and developed. The behavior and molecular mobility in this columnar liquid crystal are studied. The correlation with thermal studies allows us to understand dielectric properties as a function of physical state.

Introduction

The literature concerning the dielectric properties of polymeric liquid crystals is vast.[1–4] And yet, the relationships between intrinsic dielectric properties and physical state for DLCs remain obscure. Discotic liquid crystals (DLCs) are good models for the study of self-organising systems. Since their discovery in the 1970s,[5] DLC materials have held our attention[6,7] due to their various mesophases. Their anisotropic properties are induced by the conformation of the disk-shaped molecules and the specific intermolecular interactions. Most of the future applications are influenced by the mesomorphic properties of this molecular system. One of the major application domain for DLCs is electronic devices.[8] Since the late 1980s, organic semiconductors have been used in thin film electronic devices such as electroluminescent diodes (OLEDs), field effect transistors and solar cells. The plastic solar cells have been based on the photoinduced charge transfer at the interface between an electron-donating and an electron-accepting material. One approach to resolve this aim consists of the use of the low molecular weight compounds to create a donor/acceptor interface with two separate layers. The exciton dissociation at this interface is then followed by the electron and hole transport to the electrodes. Due to low mobility of the charge carrier in the organic thin films, the conversion efficiencies obtained are still low.

These data indicate that our researches have to look into more ordered structure like columnar liquid crystal. But since we are dealing with disk-shaped molecules we need to understand the stability of this physical structure. A complete HRTEM study has been carried out on virgin and annealed DLCs samples. Then, dipolar relaxation associated with thermal treatment will be analysed by thermostimulated current. Dielectric properties will be analysed by dynamic dielectric spectroscopy and an attempt to interpret them at a molecular level will be proposed.

Experimental section

Materials and sample preparation

Pyrene 1,3,6,8-tetracarboxylic *rac*-2-ethyl hexyl ester presents highly-ordered columnar liquid crystalline and columnar plastic crystalline phases. This liquid crystal (Fig. 1) consists of a polycyclic aromatic core surrounded by flexible side chains (the characteristic transition temperatures are dependent on the length of the side chain), and combines the good charge carrier transport of the aromatic single crystals with the good film properties of a viscous liquid. Synthesis details of this molecule were published elsewhere.[9] For TSC and DDS experiments, the sample in the liquid state, is inserted by capillarity, in μ-electrodes of 25 mm^2 area and 15 ± 3 μm thick. Contrary to TSC, DDS experiments were already performed with μ-samples

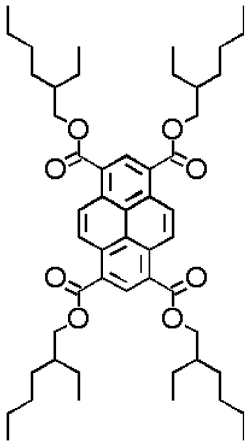

Fig. 1 Chemical structure of pyrene 1,3,6,8-tetracarboxylic *rac*-2-ethyl hexyl ester.

(or nano-samples[10,11]). DSC experiments were carried out in the bulk state.

High resolution transmission electron microscopy

Investigations were made using high resolution transmission electron microscopy (HRTEM). Electron transparent samples are required. This was achieved by depositing the liquid crystal on lacy-carbon-film-coated copper grids. The HRTEM imaging was performed using a FEI TECNAI F20 S-TWIN. The diffraction patterns were performed using the selected area diffraction (SAED) mode or by Fourier transform of the HRTEM imaging.

Standard differential scanning calorimetry

Standard differential scanning calorimetry (DSC) measurements were performed using a DSC/TMDSC 2920 set up manufactured by TA Instruments. The sample temperature was calibrated using the onset of melting of tin (T_m = 231.88 °C), indium (T_m = 156.6 °C) and cyclohexane (T_m = 6 °C) with an heating rate of $q_h = +5$ °C min^{-1}. The heat-flow was calibrated with the heat fusion of indium ($\Delta H = 28.45$ J g^{-1}), its baseline was corrected with sapphire. DSC experiments were systematically carried out over a temperature range from the equilibrium state (in order to remove the effect of previous thermal history) $T_{eq} = T_{cl} + 20$ °C down to the glassy state $T_0 = T_g - 70$ °C with a constant cooling rate q_c, and followed by a linear heating rate $q_h = +5$ °C min^{-1}. For each sample, the glass transition temperature (inflection point method) range but also the specific heat height (jump of heat capacity) were measured by Standard DSC during a heating scan ($q_h = +5$ °C min^{-1}). In order to point out thermal hysteresis of crystal-liquid/crystal transition, cooling experiments were also carried out by DSC. Samples were frozen from T_{eq} down to T_0 with a linear cooling rate ($q_c = -5$ °C min^{-1}).

Thermally stimulated currents

Complex TSC spectra and fractional polarization analysis[12,13] were carried out on a TSC/RMA Analyser. For global experiments, the sample was polarized by an electrostatic field $E_P = 400$ kV m^{-1} over $t_P = 2$ min over a temperature range from the polarization temperature $T_P = 65$ °C down to the freezing temperature $T_0 = -180$ °C. Then the field was turned off and the depolarization current was recorded with a constant heating rate ($q_h = +7$ °C min^{-1}), so that the equivalent frequency of the TSC spectrum was $f_{eq} \sim 10^{-3}$–10^{-4} Hz. TSC experiments are complementary from DDS spectroscopy on the low frequency side. For windowing experiments (ith elementary peak), the polarizing field was applied for $t_p = 2$ min at T_p^i. Then the sample was short-circuited at $T_p^i = T_p^i - \Delta T_p$ ($\Delta T_p \leq 5$ °C) and the temperature was kept constant for $t_d = t_p$. Finally, the sample was cooled at $T_0^i = T_p^i - 50$ °C, and the depolarization current was recorded in the same way as for the complex mode. Narrow poling windows ($\Delta T_p \leq 5$ °C) give elementary TSC spectra that can be analysed with the hypothesis of a single relaxation time.

Isothermal dielectric spectroscopy

Broadband dielectric measurements were performed using a NOVOCONTROL BDS400 covering a frequency range of 10^{-2} Hz–3.10^6 Hz with 10 points per decade. Experiments were carried out with a temperature range −150 °C–80 °C. Dielectric isotherm spectra were measured every 5 °C. Before each frequency scan, temperature was kept constant to within ±0.2 °C. The real ε'_T and imaginary ε''_T parts of the relative complex permittivity ε^*_T, were measured as a function of frequency F at a given temperature T. Experimental data are fitted by the Havriliak–Negami (HN) function with an additional conductivity term[14–16]:

$$\varepsilon^*_T(\omega) = \varepsilon_\infty + \frac{\varepsilon_{st} - \varepsilon_\infty}{[1 + (i\omega\tau_{HN})^{\alpha_{HN}}]^{\beta_{HN}}} - i\left(\frac{\sigma_0}{\varepsilon_{st}\omega}\right) \qquad (1)$$

where ε_∞ is the relative real permittivity at infinite frequency, ε_{st} is the relative real permittivity at null frequency, τ_{HN} is the relaxation time, ω is the angular frequency, α_{HN} and β_{HN} are the Havriliak–Negami parameters. For clarity, the electrical modulus was introduced to plot dielectric data. The dynamic dielectric modulus $M_T^*(\omega)$ is linked to permittivity by a simple mathematical relation $\varepsilon_T^*(\omega)M_T^*(\omega) = 1$. Thanks to this

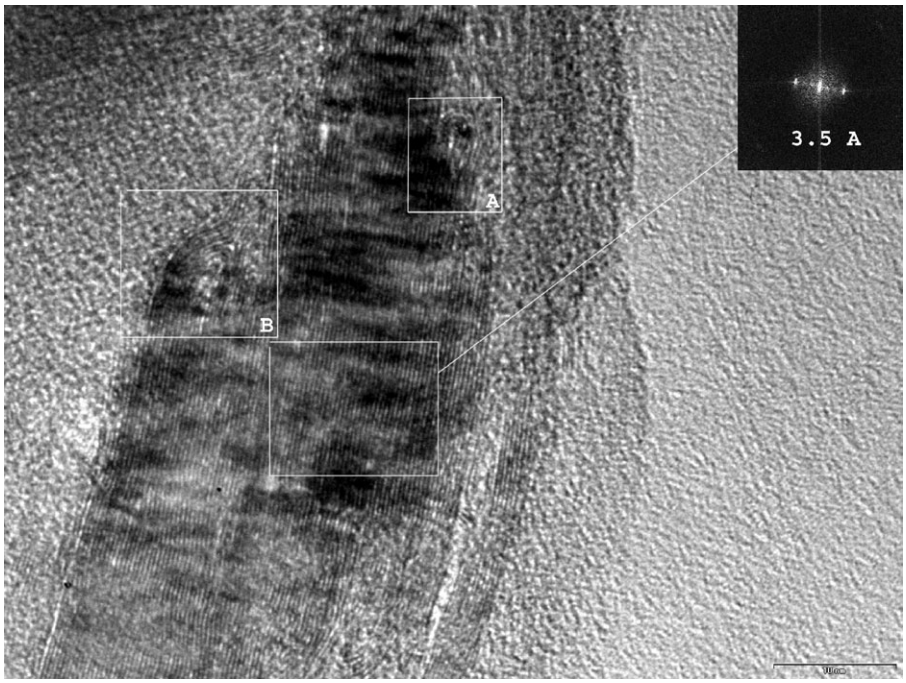

Fig. 2 HRTEM imaging of the discotic liquid crystal. inset A: columns curved until it touch another one. inset B: edge dislocation.

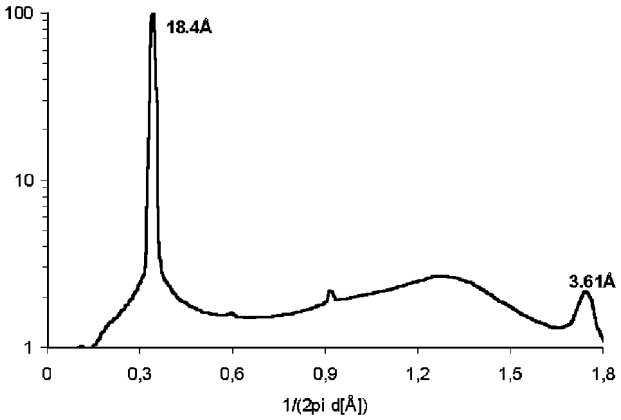

Fig. 3 X-ray diffraction pattern of pyrene 1,3,6,8-tetracarboxylic *rac*-2-ethyl hexyl ester.

relation, the imaginary part of the dielectric modulus, M_T'', is available and will be plotted.

Results

Structural dimensionality versus annealing

The HRTEM imaging of the discotic liquid crystal in Fig. 2 shows a well-disordered stack (dimension: 32 nm width × 72 nm length) which is composed of stiff and perfect domains (size: 3–5 width × 30 nm length). The planes in the stack correspond to the intra-columnar distance of 3.5 Å. This periodic disk distance in the column is determined by the Fourier transform of the HRTEM imaging.[17] This result is confirmed by the characterization of liquid crystal structure by X-ray diffraction (Fig. 3). This diagram shows that the main reflection corresponds to the spacing of an hexagonal columnar lattice (18.4 Å). The second one is characteristic of the

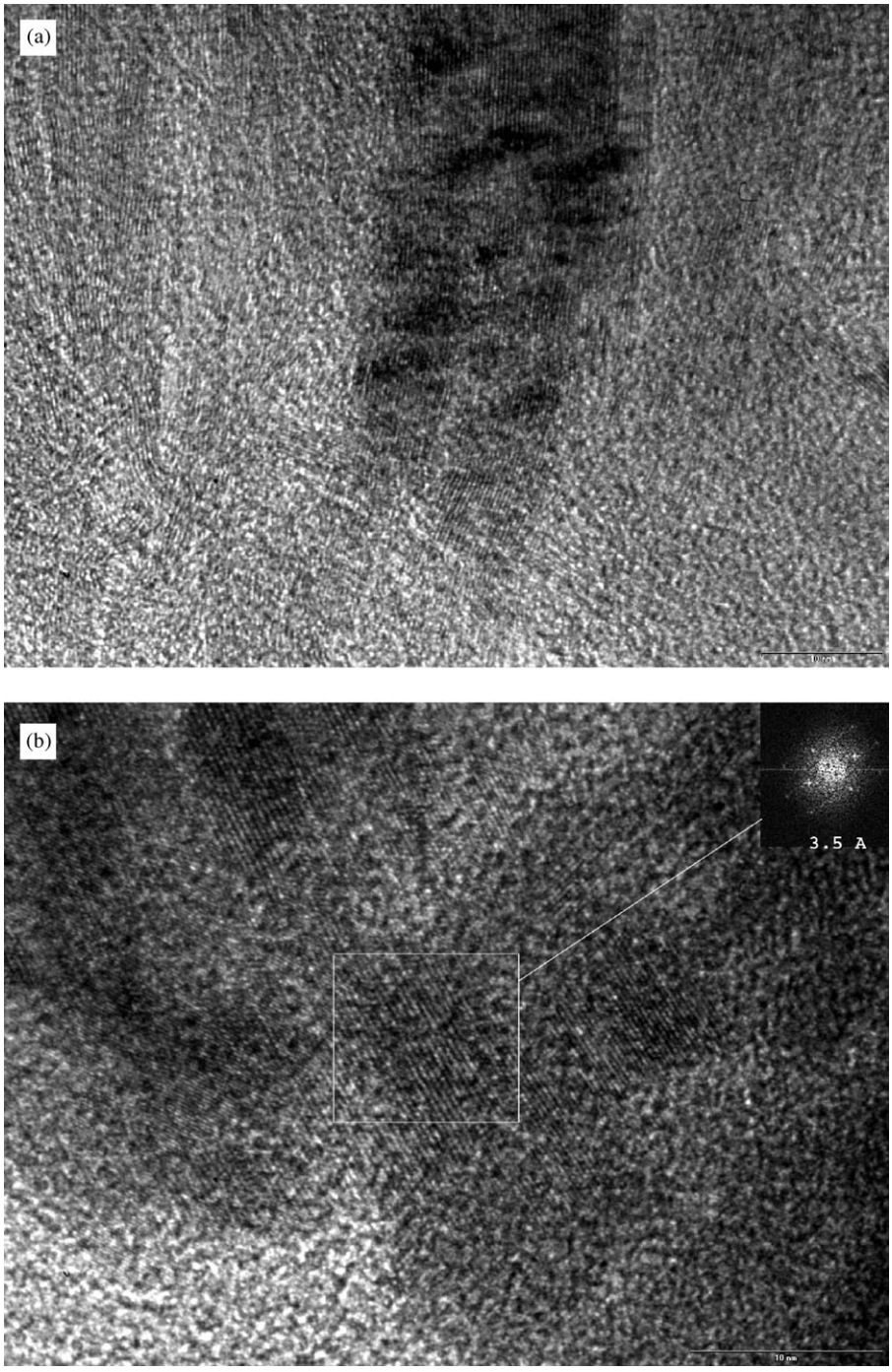

Fig. 4 Comparison of the HRTEM imaging of initial sample (top) with that of annealed ($T_a = 80$ °C, $t_a = 10$ min) sample (bottom).

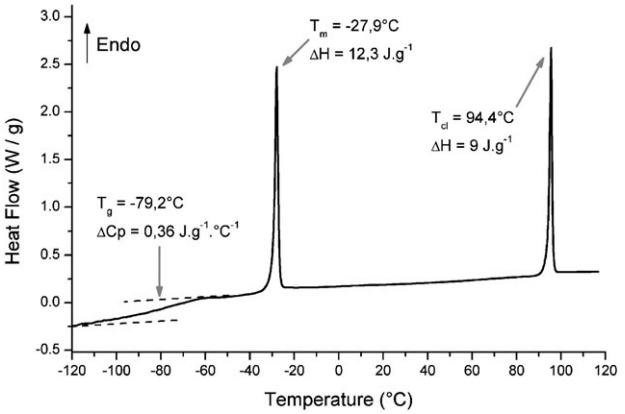

Fig. 5 DSC thermogram of pyrene 1,3,6,8-tetracarboxylic *rac*-2-ethyl hexyl ester with $q_h = +5$ °C min^{-1}.

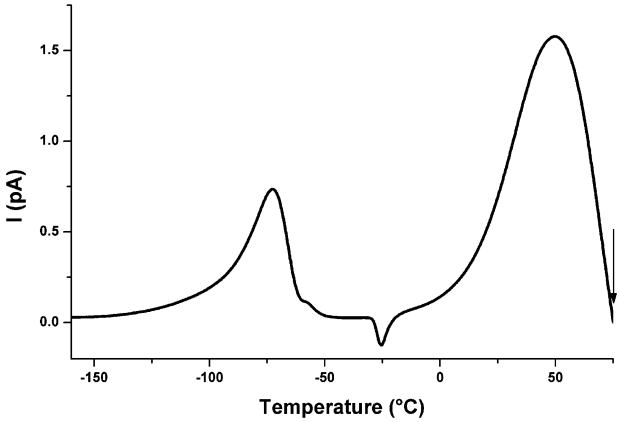

Fig. 7 Complex spectrum obtained from −180 °C to 80 °C.

distance between two disks (3.61 Å) and the broad component is due to the presence of an amorphous phase. This study confirms the liquid crystalline nature of this molecule at room temperature. In fact, the deformation in the stack is not only due to the curve of the planes (Fig. 2 inset A) but also to the edge dislocation (Fig. 2 inset B). The presence of the edge dislocation and the curve of the planes allows the reduction in the internal stresses of the liquid crystal. Nevertheless, the process of the curve 'cost' less energy what explains that this process is the most significant in the deformation mechanism. So, in a discotic liquid crystal, the columns tend to be curved until it comes to touch another column (Fig. 2 inset A). This fact is also shown in the Fig. 4 (top part) where domains are oriented in all the directions. After annealing the same sample at 80 °C, in the Fig. 4 (bottom part), the stack shows less distortions and the stiff and perfect domains size increase (size: 10 nm in width × 80 nm in length).

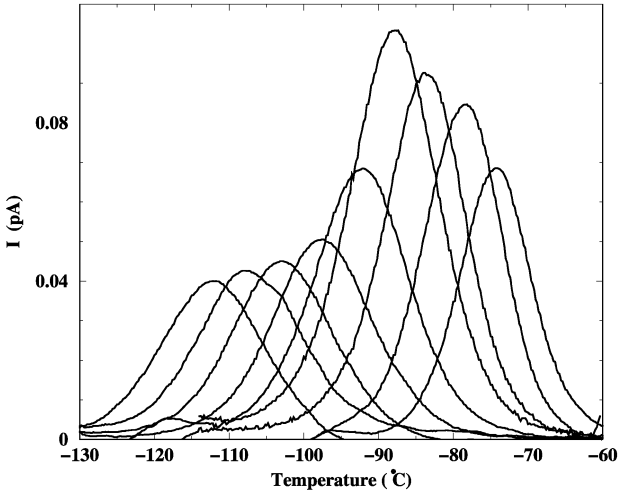

Fig. 8 Elementary spectra obtained thanks fractional polarization procedure for α mode.

Physical structure *versus* temperature

Heat flow *versus* temperature is plotted from −120 °C to 120 °C (Fig. 5). Three thermal events are shown: first one is the step of C_p ($\Delta C_p = 0.36$ J g^{-1} °C^{-1}) characteristic of glass transition, near $T_g = -79.2$ °C. ΔC_p value is the same order than linear polymers ($\Delta C_p \sim 0.5$ J g^{-1} °C^{-1}). This pseudo-second-order transition shows that glass coexists with a crystal phase. Second and third events are first order transition. Intermediate one, between the liquid and the crystal state, is probably the liquid-crystal–crystal transition at $T_m = -27.9$ °C ($\Delta H = 12.3$ J g^{-1}). In order to confirm this assumption, an heating and a cooling scan in succession are performed with the same rate $|q_c| = |q_h| = 5$ °C min^{-1}. A thermal hysteresis, for ΔT_m(heating − cooling), of approximately 20 °C is pointed out on Fig. 6. This behavior is characteristic of a displacive transition: it is a liquid-crystal–crystal transition.[18] Plane order disappears whereas columnar structure is kept: this phase transition marks the transformation from a genuine crystalline order to a mesophase, which is usually called melting. The

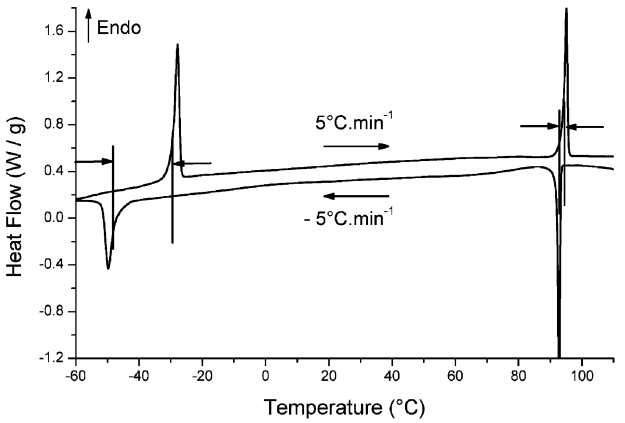

Fig. 6 Thermal hysteresis of pyrene 1,3,6,8-tetracarboxylic *rac*-2-ethyl hexyl ester with $|q_h| = |q_c| = +5$ °C min^{-1}.

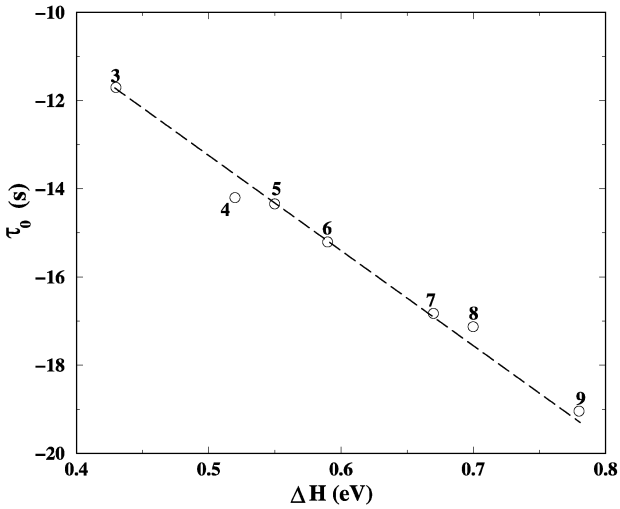

Fig. 9 τ_0 *versus* ΔH for α mode: Meyer–Neldel law.

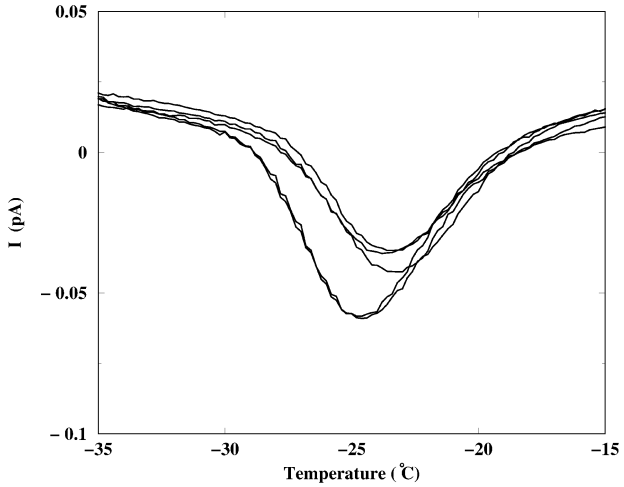

Fig. 10 Elementary spectra obtained thanks fractional polarization procedure for intermediate mode.

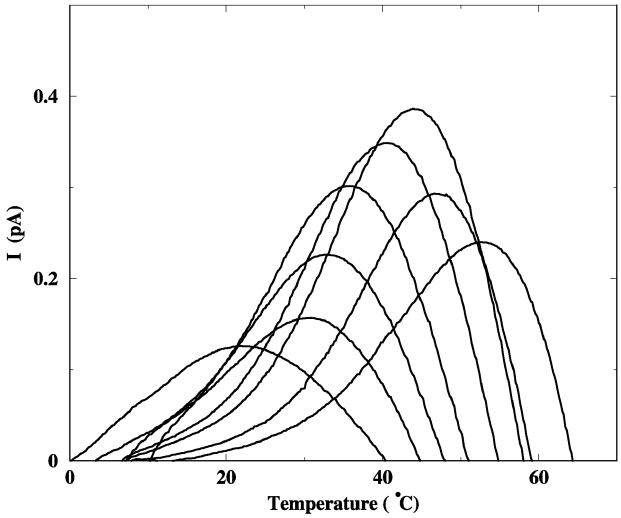

Fig. 11 Elementary spectra obtained thanks fractional polarization procedure for clearing.

clearing transition is near $T_{cl} = 94.4$ °C ($\Delta H = 9$ J.g^{-1}. At this temperature, columnar order vanishes giving rise to a liquid (*i.e.* the transition to the isotropic state). Pyrene 1,3,6,8-tetracarboxylic *rac*-2-ethyl hexyl ester is characterized by a thermotropic mesomorphism.

Dielectric properties versus temperature

A spectrum of depolarization current versus temperature is plotted on Fig. 7, obtained for polarization temperature of

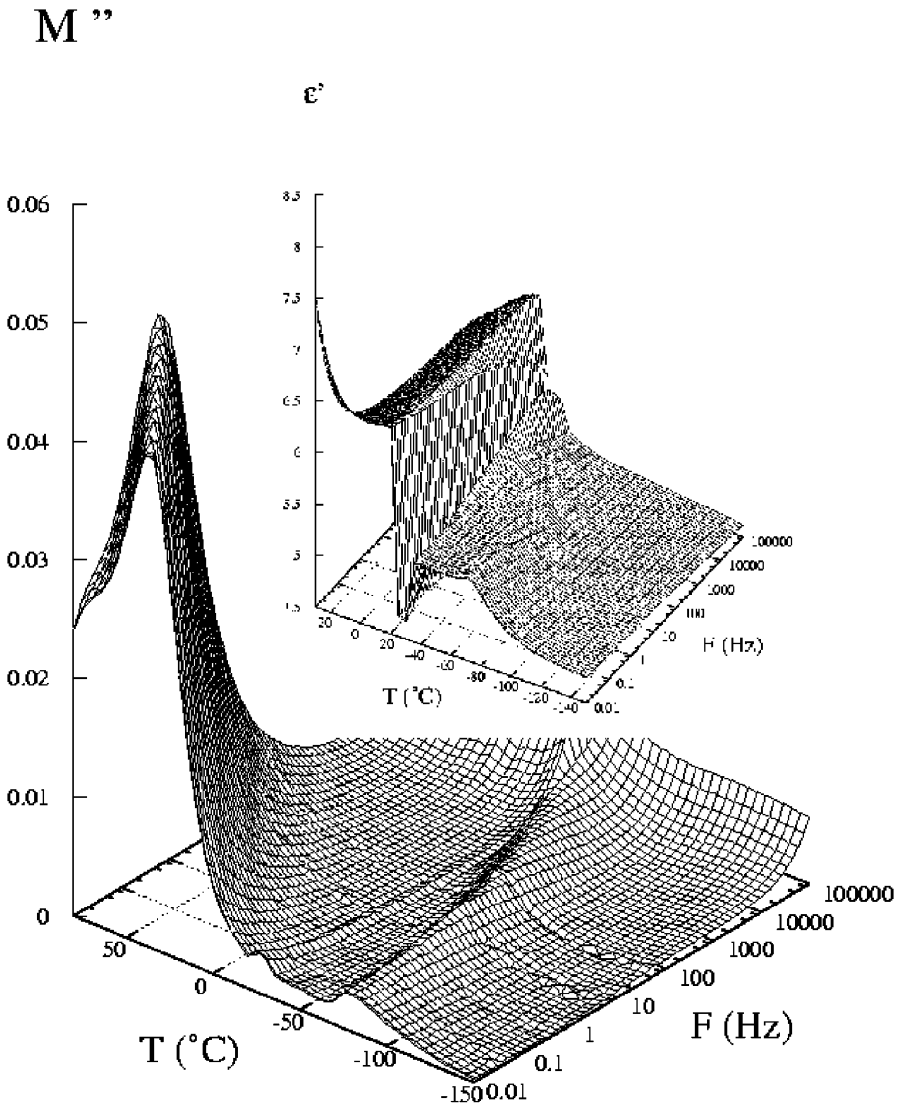

Fig. 12 Dielectric modulus surface (M'') as a function of temperature (from −150 °C to 80 °C) and frequency (from 10^{-2} Hz to 10^{+6} Hz).

T_p = 65 °C indicated by a small arrow. The maximum temperature of the relaxation mode is consistent with DSC results. We observe the dielectric manifestation of glass transition (α-mode), the melting transition and the dielectric manifestation of clearing, in order of increasing temperature. Relaxation mode associated with glass transition is observed in −125 °C/−50 °C temperature range (with $T_{max} = -72 \pm 1$ °C and $I_{max} = 0.73 \pm 0.01$ pA). The dielectric manifestation of melting transition is recorded between −30 °C/−20 °C (with $T_{max} = -25.8 \pm 0.6$ °C and $I_{max} = 0.12 \pm 0.01$ pA). This negative contribution could be interpreted as the dielectric manifestation of the Frederiks transition[18] (effect of an electric field in the mesomorphic phase); but further experiments are necessary to confirm this assumption. The main mode is shown at higher temperature with $T_{max} = 50 \pm 1$ °C and $I_{max} = 1.57 \pm 0.01$ pA. To determine the fine structure and the activation parameters, fractional polarization procedure is applied for each mode. Activation parameters are extracted and analysed. This allows us to define the enthalpy variation as a function of entropy for each isolated process. For α mode (Fig. 8), the variation of τ_0 *versus* ΔH is reported on Fig. 9. A (Meyer-Neldel) law is shown. It is characteristic of the cooperativity inherent to the dielectric manifestation of the glass transition. For the intermediate mode (Fig. 10), all elementary spectra pile up on the same temperature (near ∼−25 °C) showing a isokinetic behavior. The ultimate relaxation mode (Fig. 11) has been attributed to the precursor of clearing.

Isothermal response

Fig. 12 inset shows the real part ε'_T of the dielectric permittivity as a function of temperature and frequency. The dielectric manifestation of melting transition is pointed out as step of ε'_T ($\Delta\varepsilon'_T \sim 1.5$). This dielectric manifestation is quasi-isotherm near −27 °C. We note on low frequency part of the diagram a step near −80 °C associated with the dielectric manifestation of the glass transition. Conductivity σ appears on the low frequency tail of ε''_T. For clarity, dielectric relaxation modes are shown on a dynamic dielectric modulus representation. The imaginary part of the dielectric modulus, M_T'', is plotted on Fig. 12. A series of isotherm from −150 °C to 80 °C is represented. Three main relaxations are extracted: relaxation mode associated with the glass transition, called α mode; the melting and the clearing dielectric manifestation. The high temperature peak does not represent a pure molecular relaxation. This mode is strongly influenced by conductivity. If we zoom on the intermediate zone of the dielectric surface (Fig. 13): we follow the evolution of relaxation mode as a function of temperature and frequency. α mode has an Arrhenius-type temperature dependence with an activation energy of $E_a = 113 \pm 2$ kJ.mol^{-1}, melting mode has temperature dependence free. We note the merging between relaxation modes associated with a first order transition and a quasi-second order transition. It is also interesting to note that the activation energy for α is the same order than polymers localised β relaxation (near ∼10 − 100 kJ.mol^{-1}), suggesting that the molecular motions in this DLCs are less cooperative.

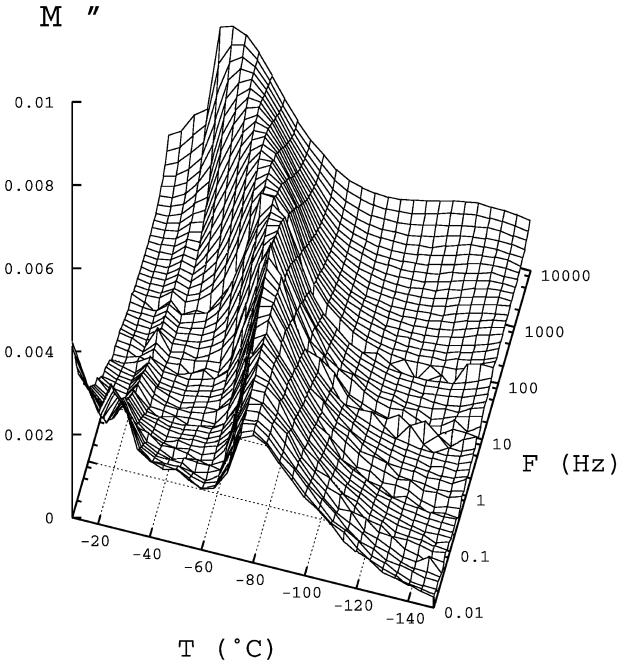

Fig. 13 Zoom in on low temperature tail of the dielectric modulus surface.

Conclusion

This combined HRTEM, DDS, TSC and standard DSC study gives us more information about behavior law and molecular mobility involved in this highly ordered columnar liquid crystal. The complete HRTEM study highlights the co-existence of an amorphous phase with perfect crystalline domains. Specific structures as curves and dislocations are exhibited. Annealing influence on alignment is confirmed. The evolution of physical structure shown through calorimetric study perfectly explains dielectric manifestation observed by DDS and TSC. At low temperatures an amorphous phase coexists with a crystalline phase. The dielectric response is dominated by the α process. Molecular mobility involves are less cooperative than polymers. Molecular motions of amorphous phase are hindered by crystalline phase. Then in the mesomorphic phase, plane order is broken. Dielectric relaxation associated to a precursor of clearing (∼40 °C before T_{cl}) and conductivity σ govern the dynamic of the mesophase. At clearing, the columnar order vanishes giving rise to a liquid. So this investigation allows us to control the dielectric behavior in a definite temperature range.

References

1 G. Williams, in *Comprehensive polymer science*, ed. D. Allen and J.C. Bevington, Pergamon Press, Oxford, 1989, vol II.
2 G. P. Simon, in *Dielectric Spectroscopy of Polymeric Materials: Fundamentals and Applications*, ed. J. P. Runt and J. J. Fitzgerald, American Chemical Society, Washington, DC, 1997, ch. 12.
3 F. Faubert, J. M. Gilli, P. Sixou, J. Dandurand and C. Lacabanne, *Mol. Cryst. Liq. Cryst.*, 1990, **178**, 133–142.
4 J. Mijovic and J.-W. Sy, *Macromolecules*, 2000, **33**, 9620–9629.
5 S. Chandrasekhar, B. K. Sadashiva and K. A. Suresh, *Pramana*, 1977, **9**, 471.
6 H. Mori, Y. Itoh, Y. Nishiura, T. Nakamura and Y. Shinagawa, *Jpn. J. Appl. Phys.*, 1997, **36**, 143–147.
7 D. Adam, P. Schuhmacher, J. Simmerer, L. Haussling, K. Siemensmeyer, K. H. Etzbach, H. Ringsdorf and D. Haarer, *Nature (London)*, 1994, **371**, 143.
8 E. W. Meijer and A. P. H. J. Schenning, *Nature*, 2002, **419** 353–354.
9 T. Hassheider, S. A. Benning, H.-S. Kitzerow, M.-F. Achard and H. Bock, *Angew. Chem., Int. Ed. Engl.*, 2001, **40**(11), 2060–2063.
10 K. Fukao and Y. Miyamoto, *Europhys. Lett.*, 1999, **46**(5), 649–654.
11 L. Hartmann, W. Gorbatschow, J. Hauwede and F. Kremer, *European Physical Journal E*, 2002, **8**(2), 145–154.
12 D. Chatain, P. Gautier and C. Lacabanne, *J. Polym. Sci., Phys. Ed.*, 1973, **1**, 1631–1640.

13 G. Teyssèdre and C. Lacabanne, *J. Phys. D: Appl. Phys.*, 1995, **28**, 1478–1487.
14 S. Havriliak and S. Negami, *J. Polym. Sci. Part C*, 1966, **14** 99–117.
15 S. Havriliak and S. Negami, *J. Polym. Sci.*, 1967, **8**, 161–210.
16 S. Havriliak, S. Negami, in *Dielectric Spectroscopy of Polymeric Materials: Fundamentals and Applications*, ed. J. P. Runt and J. J. Fitzgerald, American Chemical Society, Washington, DC, 1997, ch. 8.
17 L. Laffont, M. Monthioux and V. Serin, *Carbon*, 2002, **40** 767–780.
18 P. Papon, J. Leblond and P. H. E. Meijer, *The Physics of Phase Transitions: Concepts and Applications*, Springer-Verlag, Berlin Heidelberg, 2002.